

Stellar Variability and Distance Indicators in the Near-infrared in Nearby Galaxies. I. RR Lyrae and Anomalous Cepheids in Draco dwarf spheroidal

ANUPAM BHARDWAJ,¹ MARINA REJKUBA,² CHOW-CHOONG NGEOW,³ MARCELLA MARCONI,⁴ VINCENZO RIPEPI,⁴
ABHINNA SUNDAR SAMANTARAY,⁵ AND HARINDER P. SINGH⁶

¹*Inter-University Center for Astronomy and Astrophysics (IUCAA), Post Bag 4, Ganeshkhind, Pune 411 007, India*

²*European Southern Observatory, Karl-Schwarzschild-Straße 2, 85748, Garching, Germany*

³*Graduate Institute of Astronomy, National Central University, 300 Jhongda Road, 32001 Jhongli, Taiwan*

⁴*INAF-Osservatorio Astronomico di Capodimonte, Via Moiariello 16, 80131 Napoli, Italy*

⁵*Astronomisches Rechen-Institut, Zentrum für Astronomie, Universität Heidelberg, Mönchhofstrasse 12-14, 69120 Heidelberg, Germany*

⁶*Department of Physics and Astrophysics, University of Delhi, Delhi-110007, India*

Submitted to AJ

ABSTRACT

Draco dwarf Spheroidal galaxy (dSph) is one of the nearest and the most dark matter dominated satellites of the Milky Way. We obtained multi-epoch near-infrared (NIR, JHK_s) observations of the central region of Draco dSph covering a sky area of $\sim 21' \times 21'$ using the WIRCam instrument at the 3.6-m Canada–France–Hawaii Telescope. Homogeneous JHK_s time-series photometry for 212 RR Lyrae (173 fundamental-mode, 24 first-overtone, and 15 mixed-mode variables) and 5 Anomalous Cepheids in Draco dSph is presented and used to derive their period–luminosity relations at NIR wavelengths for the first-time. The small scatter of ~ 0.05 mag in these empirical relations for RR Lyrae stars is consistent with those in globular clusters and suggests a very small metallicity spread, up to ~ 0.2 dex, among these centrally located variables. Based on empirically calibrated NIR period–luminosity–metallicity relations for RR Lyrae in globular clusters, we determined a distance modulus to Draco dSph of $\mu_{\text{RRL}} = 19.557 \pm 0.026$ mag. The calibrated K_s -band period-luminosity relations for Anomalous Cepheids in the Draco dSph and the Large Magellanic Cloud exhibit statistically consistent slopes but systematically different zero-points, hinting at possible metallicity dependence of ~ -0.3 mag dex⁻¹. Finally, the apparent magnitudes of the tip of the red giant branch in I and J bands also agree well with their absolute calibrations with the adopted RR Lyrae distance to Draco. Our recommended $\sim 1.5\%$ precise RR Lyrae distance, $D_{\text{Draco}} = 81.55 \pm 0.98(\text{statistical}) \pm 1.17(\text{systematic})$ kpc, is the most accurate and precise distance to Draco dSph galaxy.

1. INTRODUCTION

Dwarf galaxies are the most numerous in the Universe and among the best astrophysical laboratories to study the structure of dark matter halos and the nature of dark matter (Bullock & Boylan-Kolchin 2017). According to the Lambda cold dark matter model, smaller galaxies form first in the large-scale structure formation making dwarf galaxies ideal targets to constrain galaxy formation and evolution models (see reviews by

Tolstoy et al. 2009; Battaglia & Nipoti 2022). Dwarf spheroidal (dSph) galaxies are low-luminosity ($M_V \geq -14$ mag), low-mass ($\sim 10^7 M_\odot$) early-type dwarf galaxies that host dominant old and intermediate-age stellar populations (Grebel et al. 2003; Tolstoy et al. 2009). The dSph galaxies with high mass-to-light ratios are particularly interesting systems to search for dark matter that can be inferred from analyses of their internal stellar kinematics (Mateo 1998; McConnachie 2012).

The nearest Galactic dSph galaxies ($D \lesssim 150$ kpc) are also ideal systems for detailed studies of individual stellar kinematics and their chemical abundances down to faint main sequence evolutionary phases. Aaronson (1983) measured stellar velocity dispersions of 4 Carbon

stars in Draco dSph, which were found to be significantly larger than those of globular clusters. The author inferred the mass of the Draco to be much larger than its visible content providing the first hint that dSph galaxies contain a significant amount of dark matter. Since then stellar kinematics of hundreds of individual stars including their three-dimensional internal motions, have established Draco dSph as one of the most dark matter dominated satellites of the Milky Way (e.g., Read et al. 2018; Massari et al. 2020; Battaglia & Nipoti 2022).

Distance of a galaxy is the fundamental ingredient for modeling of its dynamical history, formation and evolution. Nevertheless, despite extensive studies of resolved stellar populations in Draco (e.g., Grillmair et al. 1998; Aparicio et al. 2001; Cioni & Habing 2005; Ségal et al. 2007; Kinemuchi et al. 2008; Walker et al. 2015; Muraveva et al. 2020) the distance estimates to this dSph available in the literature have a considerable scatter, which makes it poorly constrained. The distance modulus to Draco dSph ranges between 19.35 and 19.85 mag with typical uncertainties of 5 – 7% (see Section 5). The majority of previous distance determinations are based on horizontal branch stars and RR Lyrae (RRL) visual magnitude–metallicity ($M_V - [\text{Fe}/\text{H}]$) relations (Stetson 1979; Bellazzini et al. 2002; Kinemuchi et al. 2008; Muraveva et al. 2020). However, these empirical relations may not be linear over the entire metallicity range, and are very sensitive to evolutionary effects because evolved RRL stars exhibit higher luminosities (Caputo et al. 2000; Beaton et al. 2018; Bhardwaj 2020). Furthermore, significant uncertainties in metallicity and reddening can lead to systematic errors of the order of 5% in distance measurements based on optical data for RRL stars.

High-precision distances based on RRL and Anomalous Cepheid (ACEP) variable stars can be obtained at near-infrared (NIR) wavelengths where these pulsating stars exhibit tight period–luminosity (PL) and period–Wesenheit (PW) relations (Longmore et al. 1986; Ripepi et al. 2014; Bhardwaj 2022; Monelli & Fiorentino 2022, and references therein). At optical bands, variable star search in Draco dSph dates back to Baade & Swope (1961), who discovered more than 260 variables including 133 RRL stars, which were used in several subsequent studies to improve their identification and classification (Zinn & Searle 1976; Nemec 1985). Modern VI band photometric observations of variable stars in Draco dSph were provided by Kinemuchi et al. (2008) including 270 RRL and 9 ACEP stars. Muraveva et al. (2020) revisited RRL population in Draco dSph using *Gaia* data investigating their $M_G - [\text{Fe}/\text{H}]$ relations. However,

time-series observations for variable stars in Draco dSph have not been carried out so far at infrared wavelengths. We note that random-epoch NIR photometry of variable stars in several other Local Group galaxies have been utilized by the Araucaria project to determine their precise distances (Gieren et al. 2005; Karczmarek et al. 2021).

This paper is the first in a series of Stellar VARIability and Distance Indicators in the Near-infrared (SVADhIN¹) project, which aims to obtain NIR multi-epoch observations of variable stars in nearby Local Group galaxies. Homogeneous time-series NIR photometry of RRL and ACEP variables in the pilot Draco dSph will enable determination of a precise distance to this galaxy. The observations and data reduction are presented in Section 2. Light curves and PL relations for variable stars are discussed in Sections 3 and 4. The distance to Draco dSph is presented in Section 5 and the results are summarized in Section 6.

2. DATA AND PHOTOMETRY

2.1. Observations and data reduction

Multi-epoch NIR observations of Draco dSph were obtained using the WIRCam instrument (Puget et al. 2004) mounted on the 3.6-m Canada-France-Hawaii Telescope (CFHT). The NIR camera, WIRCam, is an array of four 2048×2048 HgCdTe HAWAII-RG2 detectors that are arranged in a 2×2 grid with gaps of $45''$ between adjacent detectors. The pixel scale is $0.3''$ pixel⁻¹ resulting in a wide field of view of $\sim 21' \times 21'$. The multi-epoch JHK_s observations were collected in the queue mode on 6 different nights between Feb 15, 2022 and Aug 8, 2022. We had requested 10 JK_s epochs and 3 H band epochs, but finally received 10, 5, and 8 epochs in J , H , K_s , respectively, due to a combination of the target’s visibility, weather constraints and priority among allocated projects during the scheduled WIRCam runs. Each J band epoch consisted of 20 dithered images with 30s exposure times, while 40 dithered images were taken in HK_s each with 25s exposure time. A summary of all the epochs in JHK_s -bands is listed in Table 1.

The pre-processed science images were downloaded from the IDL Interpreter of the WIRCam Images (‘I²iwi’) preprocessing pipeline at CFHT which incorporates detrending (dark subtraction, flat-fielding) and initial sky subtraction. We first used WeightWatcher

¹ SVADhIN refers to freedom or independence in Hindi and Sanskrit languages.

² <https://www.cfht.hawaii.edu/Instruments/Imaging/WIRCam/IwiVersion2Doc.html>

Table 1. Log of NIR observations.

Date	MJD	FWHM	AM	ET	N_f
<i>J</i> -band					
2022-02-15	59625.6707	1.73	1.38	30	20
2022-07-04	59764.4427	1.54	1.36	30	20
2022-07-04	59764.5053	1.85	1.62	30	20
2022-07-05	59765.2795	1.69	1.41	30	21
2022-07-05	59765.4126	1.65	1.30	30	20
2022-07-05	59765.4818	1.76	1.51	30	20
2022-07-06	59766.3045	1.35	1.33	30	20
2022-07-06	59766.4590	1.83	1.43	30	18
2022-08-07	59798.3306	1.46	1.32	30	20
2022-08-08	59799.2769	1.40	1.27	30	20
<i>H</i> -band					
2022-07-04	59764.4736	1.56	1.46	25	40
2022-07-05	59765.4449	1.67	1.37	25	40
2022-07-06	59766.2576	1.80	1.48	25	28
2022-07-06	59766.4724	2.00	1.48	25	40
2022-08-07	59798.3450	1.46	1.35	25	40
<i>K_s</i> -band					
2022-07-04	59764.4255	1.47	1.32	25	46
2022-07-04	59764.4895	1.60	1.53	25	40
2022-07-05	59765.2637	1.53	1.46	25	40
2022-07-05	59765.3360	1.61	1.29	25	46
2022-07-05	59765.3971	1.62	1.28	25	40
2022-07-05	59765.4654	1.61	1.44	25	40
2022-07-06	59766.4436	1.61	1.38	25	40
2022-08-07	59798.3607	1.38	1.39	25	40

NOTE—MJD: Modified Julian Date (JD−2,400,000.5).

FWHM: Measured median full width at half maximum using **SExtractor**. AM: Median airmass. N_f : Number of dithered frames on target per epoch. ET: Exposure time (in seconds) for each dithered frame.

(Marmo & Bertin 2008) to create weight maps for each pre-processed image thereby masking bad pixels in the WIRCam mosaic. These weight maps were used along with the images in **SExtractor** (Bertin & Arnouts 1996) to generate a catalogue of sources matching those from the Two Micron All Sky Survey (2MASS) Point Source Catalog (Skrutskie et al. 2006). These matched source catalogues were used to obtain astrometric solution for each pre-processed image using **SCAMP** (Bertin 2006). We note that the **SCAMP** also scales the flux of each detector with their magnitude zero-points and performs an internal photometric calibration against 2MASS. Finally with the astrometric solutions, the dithered images at a given epoch were median-combined using **SWARP**

(Bertin et al. 2002) at the instrument pixel scale for photometric data reduction. These co-added median combined images for each filter independently and for each epoch were used as input for photometry of point sources.

2.2. Point-spread function photometry

The point-spread function (PSF) photometry on WIRCam images has been discussed in detail in Bhardwaj et al. (2020) and Bhardwaj et al. (2021a) for Messier 3 and Messier 15 globular clusters. In brief, the standard DAOPHOT/ALLSTAR (Stetson 1987) and ALLFRAME (Stetson 1994) routines were used for PSF photometry. Initially, an aperture photometry was performed on all sources with brightness above 5σ of the detection threshold using DAOPHOT. An empirical PSF was generated from 200 bright, isolated, non-saturated stars excluding those around the corners of each detector. These PSFs were used to obtain ALLSTAR photometry for all sources in a given image. For the ALLFRAME run, a common reference-star list was obtained from a median-combined image using the best-seeing epoch in JK_s filters (Aug 8, 2022, FWHM \sim 1.4). The frame-to-frame transformations were derived between the reference star-list and all epoch images using DAOMATCH/DAOMASTER. These transformations together with the reference star-list were used for the PSF photometry in ALLFRAME, which performs profile fitting of all sources across all the frames, simultaneously. The output photometry in all the frames were internally calibrated using 50 secondary standards present in each frame in a given NIR filter. These non-variable secondary standards were chosen to have small photometric variability and were used to correct for the epoch-dependent frame-to-frame zero-point variations obtaining final catalog with instrumental JHK_s photometry.

The photometric calibration was performed by matching the instrumental photometry with 2MASS catalog within a search radius of $1.0''$. We found 556 common sources, which were restricted to 186 stars with the best-quality photometric flags in 2MASS, small uncertainties (< 0.1 mag), and spatial location away from the detector edges. The instrumental magnitudes were corrected for a fixed zero-point offset to convert into 2MASS system. The zero-point offsets in JHK_s bands were determined accurately with uncertainties of 0.01 mag in all three filters. These 2MASS standards covered a typical color-range of $0.3 < (J - K_s) < 1.0$ mag, and no statistically significant variations were found in the zero-point offsets within this color range. A narrow color-range ($\Delta(J - K_s) \lesssim 0.7$ mag) and large uncertainties in colors (up to 0.15 mag) prevented an accurate and pre-

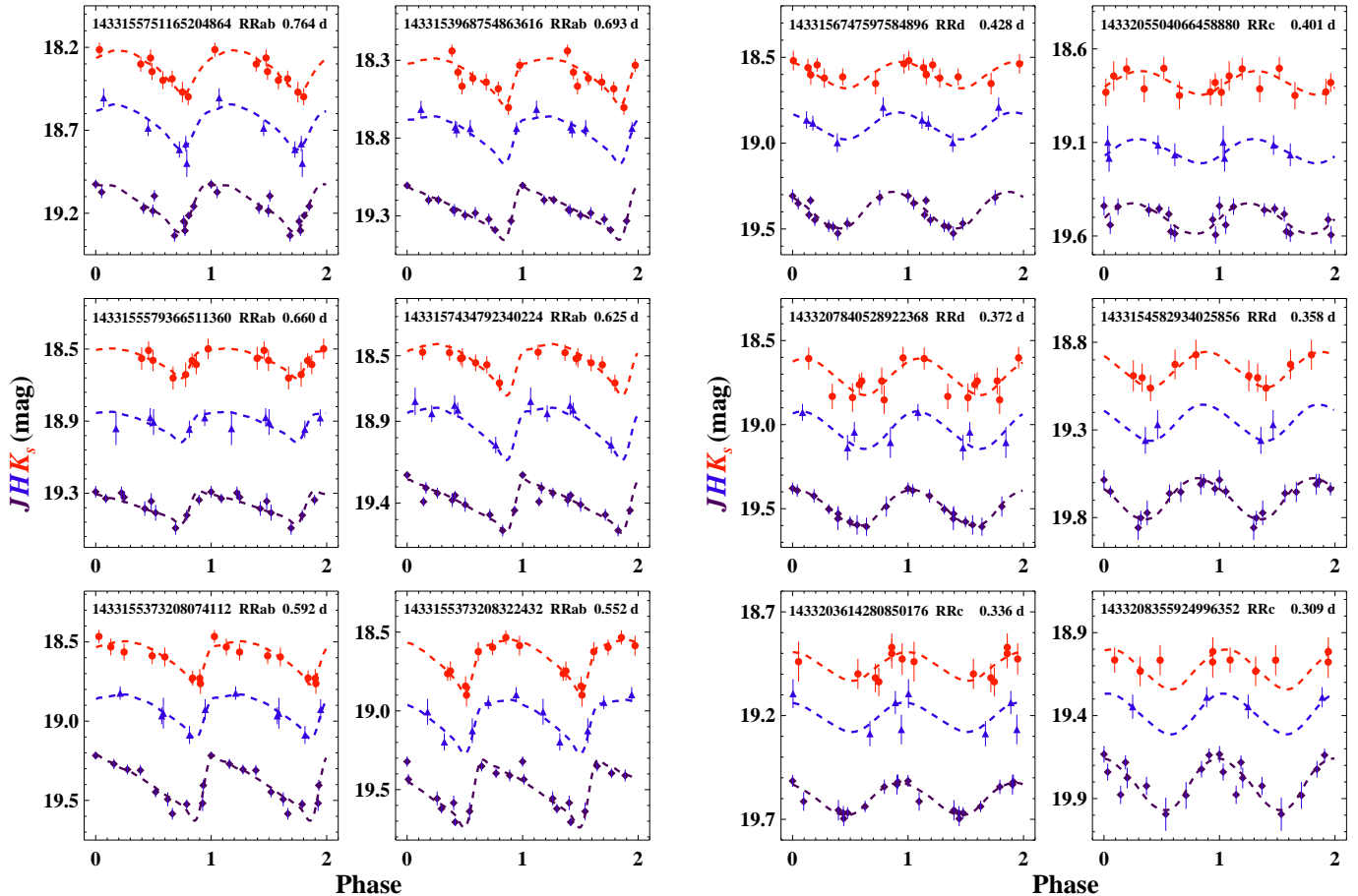


Figure 1. Example phased light curves of RR Lyrae stars in NIR bands covering the entire range of periods in our sample. *Left:* RRab stars. *Right:* RRc/RRd stars. The J -band (blue) and K_s -band (red) light curves are offset for clarity by $+0.2$ mag and -0.3 mag, respectively. The dashed lines represent the best-fitting templates to the data in each band. The *Gaia* DR3 star ID, variable subtype, and the pulsation period are included at the top of each panel.

cise quantification of the color-coefficient in the transformation. Therefore, we did not apply color corrections. We estimate an uncertainty of 0.01 mag in photometry given the small color range of RRL and ACEP stars ($\Delta(J - K_s) \lesssim 0.5$ mag).

3. VARIABLE STARS IN DRACO

We used an initial list of 379 variable stars towards Draco dSph compiled by Muraveva et al. (2020). The compilation includes positions, periods, and variability types from several different literature studies and *Gaia* DR2 data (see Muraveva et al. 2020, for details). This initial list included 336 RRL and 9 ACEP variables, which were cross-matched with our NIR photometry catalog within $1''$ tolerance. We recovered all 217 variables within the field of view of WIRCam consisting of 212 RRL - 173 fundamental mode (RRab), 23 first-overtone (RRc), and 15 mixed-mode (RRd) variables, and 5 ACEP variable stars. The light curves in JHK_s

bands were extracted for these 217 variables in Draco, which were phased using the adopted periods from the list of Muraveva et al. (2020). The mixed-mode (RRd) variables were phased with their dominant first-overtone periods.

3.1. Template-fitted light curves

The phased light curves were fitted with NIR templates for RRL stars from Braga et al. (2019). We fitted all three sets of RRab templates from Braga et al. (2019) to their observed NIR light curves irrespective of the periods. The J band reference epoch corresponding to the maximum light was used to phase all three JHK_s band light curves. Therefore, we solved for the mean-magnitude, peak-to-peak amplitude, and a phase offset in the case of J band. The measured phase offset was kept fixed for the template-fitting in HK_s bands. In the case of K_s band, mean-magnitudes and amplitudes were determined simultaneously. However, we only solved for

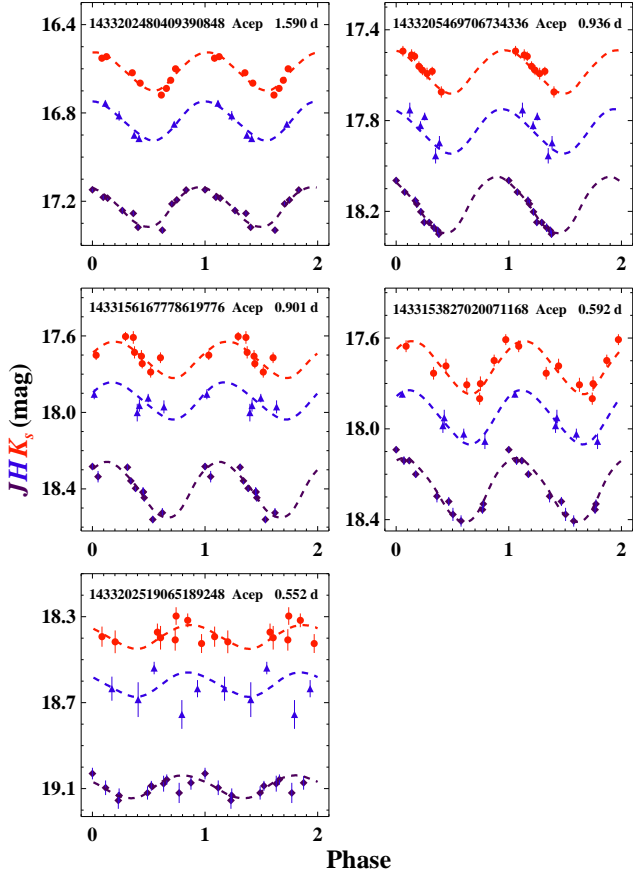


Figure 2. Same as Fig. 1 but for ACEP stars. The J -band (blue) and K_s -band (red) light curves are offset for clarity by $+0.1$ mag and -0.2 mag, respectively.

the mean magnitudes in H band assuming the amplitude to be similar to that in the K_s band. This is a reasonable approximation since the light curve shape in H and K_s bands do not change significantly and there are not enough H band epochs to independently constrain the amplitudes.

Fig. 1 displays template-fitted light curves of RR Lyrae stars in JHK_s bands covering the entire period range. The phased light curves of RRab stars are well sampled in JK_s bands while the templates reproduce the light curve variations of few epochs in the H band. In the case of RRc/RRd, we use the single near-sinusoidal template provided by Braga et al. (2019) for all stars. The sinusoidal set of JHK_s templates was also used for the ACEP light curves since there are no NIR templates available for these stars. Fig. 2 shows template-fitted light curves for ACEP stars. The faint and low-amplitude RRc stars exhibit larger scatter in their light curves while the brighter ACEP show distinct and clear light curve variations. The best-fitting light curve templates for RRL and ACEP stars were

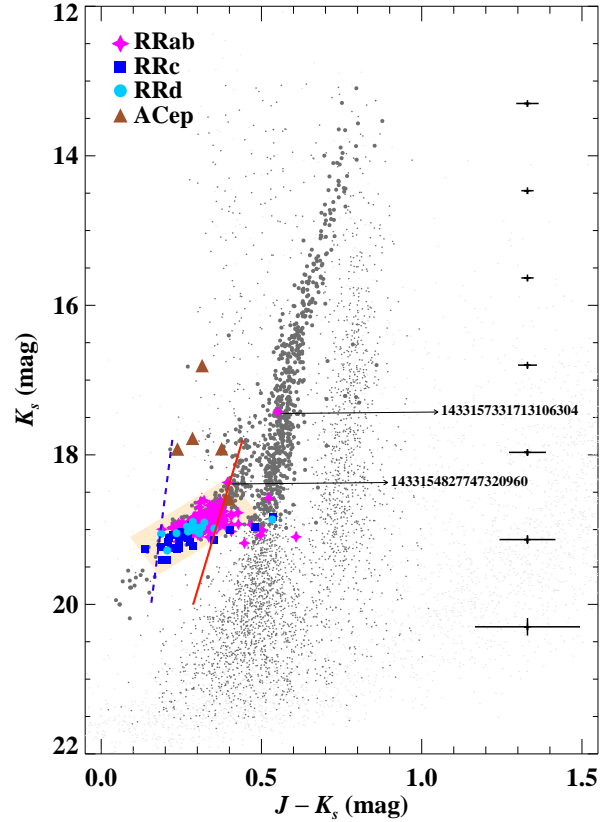


Figure 3. NIR color-magnitude diagram for Draco dSph in $(J - K_s), K_s$ (small grey dots). The larger symbols represent likely Draco members based on their proper-motions in *Gaia* DR3. Variable stars studied in this work are also overplotted with their mean magnitudes and colors. The theoretically predicted instability strip boundaries - fundamental red edge (solid red line) and first-overtone blue edge (dashed blue line) are taken from Marconi et al. (2015). On the right the representative $\pm 3\sigma$ error bars are shown as a function of magnitude and color.

used to derive their intensity-weighted mean magnitudes and colors. The median value of photometric uncertainties for the intensity-weighted mean magnitudes of RRL and ACEP are 0.036/0.045/0.034 mag and 0.030/0.034/0.022 mag in $J/H/K_s$, respectively. Table 2 lists the pulsation properties of variable stars in Draco dSph.

3.2. Color-magnitude diagrams

Fig. 3 displays NIR color-magnitude diagram for Draco dSph galaxy based on ~ 4000 point-like sources. The magnitudes and colors for all sources were corrected for extinction adopting a color-excess value of $E(B - V) = 0.027$ mag (Schlegel et al. 1998) following previous works by Muraveva et al. (2020) and Kinemuchi et al. (2008). We adopted the reddening

Table 2. NIR pulsation properties of variable stars in Draco dSph.

ID	RA	Dec	P	Type	Mean magnitudes (m_λ)			σ_{m_λ}		
					J	H	K_s	J	H	K_s
	deg.	deg.	days		mag			mag		
1433161145644413696	260.222875	57.951278	0.68171	RRab	19.126	18.772	18.760	0.033	0.046	0.033
1433203889158772608	259.898833	57.975611	0.68418	RRab	19.086	18.799	18.749	0.037	0.059	0.028
1433153620861638528	259.858833	57.814250	0.68939	RRab	19.113	18.830	18.794	0.022	0.069	0.026
1433153968754863616	259.840833	57.855944	0.69306	RRab	19.057	18.758	18.681	0.026	0.022	0.035
1433204237051138304	260.078958	58.010528	0.69485	RRab	19.094	18.739	18.780	0.047	0.061	0.040
1433154789092499584	260.087792	57.871944	0.73202	RRab	19.004	18.663	18.698	0.020	0.023	0.028
1433203859095469440	259.872750	57.973806	0.74363	RRab	19.015	18.730	18.676	0.023	0.028	0.021
1433155751165204864	260.025042	57.896944	0.76413	RRab	18.934	18.644	18.613	0.033	0.067	0.039
1433161832839184512	260.162458	57.959000	0.79061	RRab	18.988	18.672	18.616	0.016	0.040	0.016
143315616778619776	260.074110	57.952090	0.90087	Acep	18.295	17.936	17.919	0.031	0.023	0.022
1433205469706734336	259.783690	57.976370	0.93649	Acep	18.064	17.844	17.779	0.030	0.044	0.022
1433202480409390848	259.900190	57.904310	1.59027	Acep	17.121	16.833	16.806	0.023	0.034	0.027

NOTE—The *Gaia* DR3 source ID are provided in the first column.
 (This table is available in its entirety in machine-readable form.)

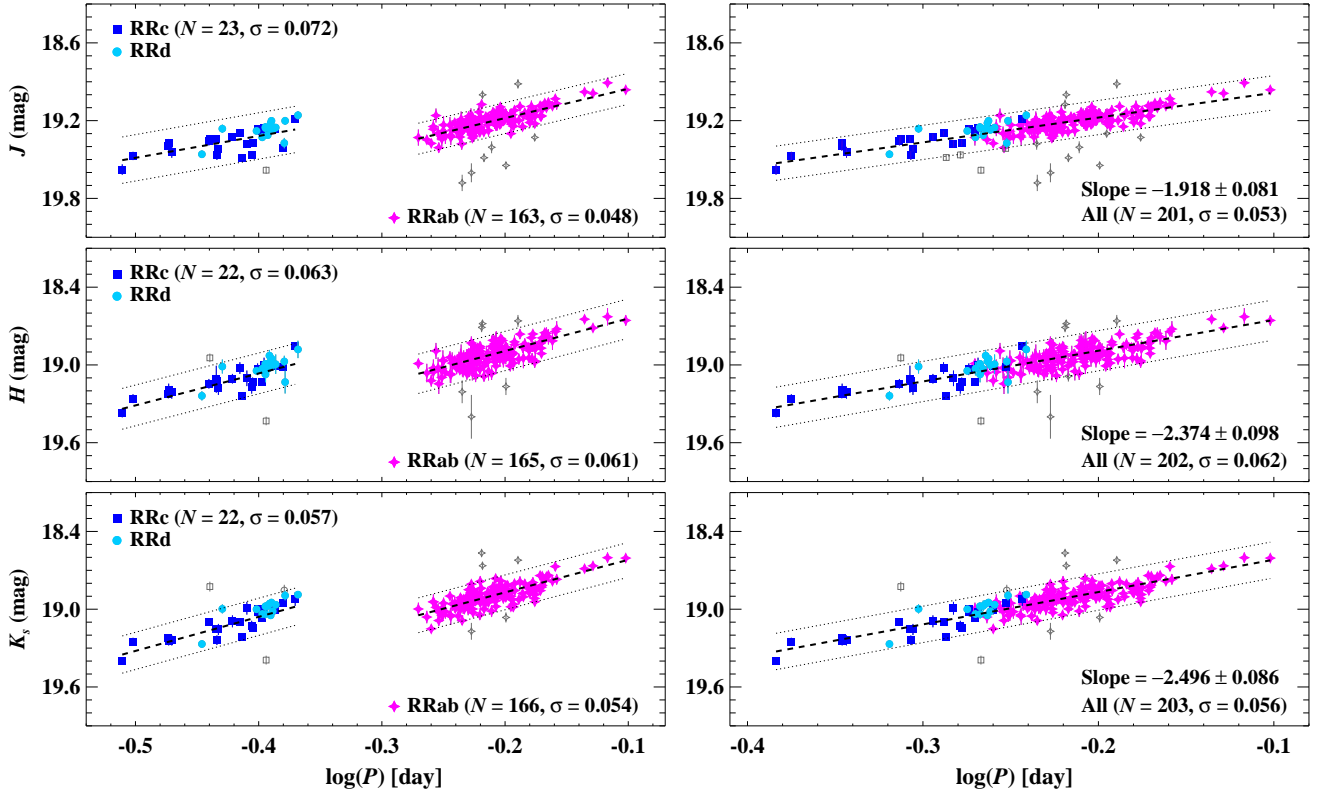


Figure 4. Near-infrared period-luminosity relations for RRab and RRc stars (left) and all RRL stars (right) in J (top), H (middle), and K_s (bottom). In the right panels, the periods for the RRc stars have been shifted to their corresponding fundamental-mode periods, as explained in the text. The grey symbols represent outliers removed iteratively during the fitting procedure. The dashed lines represent best-fitting linear regressions over the period range under consideration, while the dotted lines display $\pm 2.5\sigma$ offsets from the best-fitting PLRs.

law of Cardelli et al. (1989) and determined extinction in NIR using $A_{J/H/K_s} = 0.94/0.58/0.39E(B - V)$. Bhardwaj et al. (2023a) adopted the same reddening coefficients to provide calibrated NIR period-luminosity-metallicity (PLZ) and period-Wesenheit-metallicity (PWZ) relations for RRL stars which will be used for the distance measurement in Section 5.

The sources in the color-magnitude diagram were also cross-matched with the *Gaia* DR3 catalogue (Gaia Collaboration et al. 2023) to extract proper motions of ~ 2300 stars. The majority of fainter stars ($K_s > 19$ mag) do not have proper motions. We found mean proper motions along the right ascension and declination axes to be 0.027 ± 0.014 and -0.220 ± 0.014 mas/yr with a scatter of 1.02 and 0.94 mas/yr, respectively after restricting the sample to good astrometry (renormalized unit weight error < 1.4) and photometry ($\sigma_{JHK_s} < 0.3$ mag). These mean proper motions are in good agreement with previous determinations based on *Gaia* data (e.g., 0.044 ± 0.005 and -0.188 ± 0.006 mas/yr in Pace et al. 2022). The proper-motion cleaned color-magnitude diagram (in larger grey symbols) clearly exhibits well-populated horizontal and red giant branches.

The distribution of variable stars in the color-magnitude diagram is also shown in Fig. 3. The abundant RRL population is distinctly evident at the horizontal branch. The predicted boundaries of the instability strip were taken from Marconi et al. (2015) based on RRL pulsation models. The instability strip boundaries were offset by a distance modulus of 19.53 ± 0.07 mag (Muraveva et al. 2020). Majority of RRL stars occupy the location between the predicted fundamental red edge and the first-overtone blue edge. One of the brightest RRL (DR3-1433157331713106304) does not show any variability in its light curve within the photometric errors while NIR light curves of DR3-1433154827747320960 exhibit large scatter. Most variables located in the color-magnitude diagram beyond the predicted edges of the instability strip are still consistent with expectations. These variables exhibit larger scatter in J and/or K_s light curves, and their colors are within 1σ scatter from the instability strip boundaries.

4. VARIABLE STARS AS DISTANCE INDICATORS

4.1. RR Lyrae PL and PW relations

The extinction-corrected intensity-weighted mean magnitudes for RRL stars were used to derive PL relations in NIR bands for the first time in Draco dSph. Three different samples of RRL stars were considered: (1) RRab variables only, (2) RRC stars only, and (3) all RRL stars where the dominant first-overtone periods

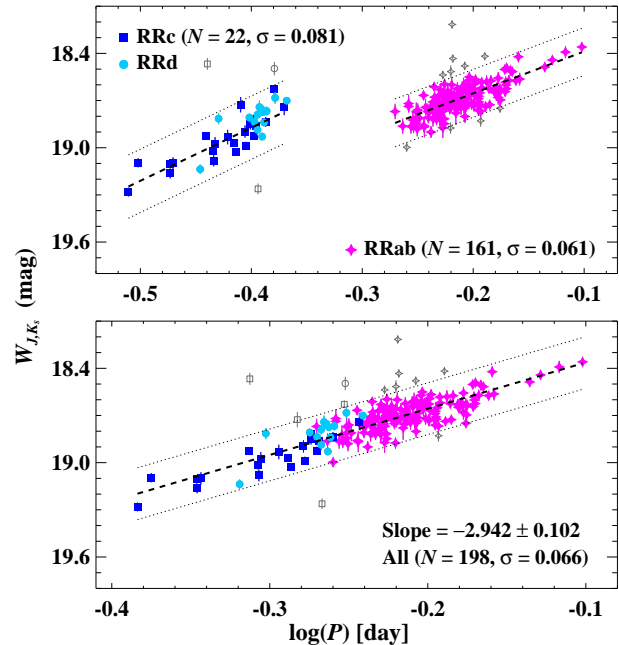


Figure 5. Same as Fig. 4, but for W_{J,K_s} period-Wesenheit relation for RRab and RRC stars (top) and all RRL stars (bottom).

were used for RRd stars. The first-overtone periods were fundamentalized using $\log(P_{\text{RRab}}) = \log(P_{\text{RRC/RRd}}) + 0.127$ (Coppola et al. 2015; Braga et al. 2022). Assuming that the PL relations are linear over the entire period range, the following relation was fitted to the data:

$$m_\lambda = a_\lambda + b_\lambda \log(P), \quad (1)$$

where m_λ is the extinction-corrected mean magnitude in JHK_s bands, and a_λ and b_λ give the slope and zero-point of the PL relation. We fitted a linear regression iteratively removing the single largest 2.5σ residual of the PL relation under consideration.

Fig. 4 displays PL relations for RRL stars in JHK_s bands. It is evident that the scatter in the PL relations for all RRL sample is small (~ 0.05 mag) and comparable to those seen in globular clusters (Bhardwaj et al. 2023a). The scatter typically results from the intrinsic width of the instability strip, a possible metallicity scatter, and photometric uncertainties on mean-magnitudes. It can be noted that the dispersion in the H -band PL relation is relatively larger than in JK_s bands because the mean-magnitudes in H band are based on a smaller number of epochs. Since the metallicity coefficients of RRL PLZ relations in the NIR are of the order of ~ 0.2 mag/dex (Marconi et al. 2015; Bhardwaj et al. 2023a), the small dispersion of ~ 0.05 mag in NIR PL relations suggests no statistically significant scatter in $[\text{Fe}/\text{H}]$ for

RRL in Draco dSph. If we assume the intrinsic width of the instability strip of 0.03 mag (e.g., RRL PL relations in M53, Bhardwaj et al. 2021b) and attribute the remaining scatter of 0.04 mag to metallicity, then the dispersion in $[\text{Fe}/\text{H}]$ is expected to be ~ 0.2 dex in these centrally located RRL stars.

Table 3 lists PL relations for different samples of RRL stars. The slopes of PL relations become steeper moving from J to K_s , as typically seen for RRL stars. The slopes are best-constrained for the global sample of all RRL stars. The slopes of RRL PL relations in Draco dSph are in good agreement with the slopes of NIR PLZ relations for RRL in globular clusters (-1.83 ± 0.02 in J , -2.29 ± 0.02 in H , and -2.37 ± 0.02 in K_s , Bhardwaj et al. 2023a) within their 1.5σ uncertainties.

We also derived PW relations for RRL stars in Draco dSph. The following reddening-free Wesenheit magnitudes (Madore 1982) were derived in NIR filters: $W_{J,H} = H - 1.63(J - H)$, $W_{J,K_s} = K_s - 0.69(J - K_s)$, $W_{H,K_s} = K_s - 1.92(H - K_s)$, similar to Bhardwaj et al. (2023b). These Wesenheit magnitudes were used in eqn. (1) to derive PW relations, and the results of the best-fitting linear regression are listed in Table 3. Fig. 5 displays W_{J,K_s} PW relation for RRL stars, which is best-constrained among these empirical relations. The scatter in the PW relations is larger than PL relations, in particular, in the Wesenheit magnitudes involving H -band. This is due to larger uncertainties in $J - H$ and $H - K_s$ colors because of lower number of epochs used to determine H -band RRL mean magnitudes. The larger color-coefficients and the uncertainties in colors contribute to the significantly increased scatter in $W_{J,H}$ and W_{H,K_s} PW relations as compared to PL relations. Nevertheless, the slopes of PW relations are in agreement with those of RRL in globular clusters (Bhardwaj et al. 2023b).

4.2. Anomalous Cepheid PL and PW relations

We also investigated NIR PL relations for a small sample of 5 ACEP variables in Draco dSph. Previously, K_s -band PL relations for ACEP have been investigated only in the Large Magellanic Cloud (LMC, Ripepi et al. 2014), and no other empirical PL relations are available for these variables at NIR wavelengths. Ripepi et al. (2014) derived K_s -band PL relations for both fundamental and first-overtone mode ACEP variables. Therefore, to identify the pulsation mode of ACEP in Draco dSph, we compared the location of their PL relations with ACEPs in the LMC. The distance moduli $\mu_{\text{Draco}} = 19.53 \pm 0.07$ mag (Muraveva et al. 2020) and $\mu_{\text{LMC}} = 18.48 \pm 0.03$ mag (Pietrzyński et al. 2019)

Table 3. Near-infrared PL and PW relations of RRL stars in Draco dSph.

Band	Type	a_λ	b_λ	σ	N
J	RRab	18.728 ± 0.024	-2.260 ± 0.118	0.048	163
	RRc	18.645 ± 0.183	-1.684 ± 0.437	0.072	23
	All	18.793 ± 0.018	-1.918 ± 0.081	0.053	201
H	RRab	18.393 ± 0.033	-2.499 ± 0.161	0.061	165
	RRc	18.079 ± 0.158	-2.465 ± 0.374	0.063	22
	All	18.416 ± 0.022	-2.374 ± 0.098	0.062	202
K_s	RRab	18.368 ± 0.028	-2.511 ± 0.135	0.054	166
	RRc	18.007 ± 0.141	-2.629 ± 0.330	0.057	22
	All	18.368 ± 0.019	-2.496 ± 0.086	0.056	203
$W_{J,H}$	RRab	17.822 ± 0.046	-3.074 ± 0.226	0.092	156
	RRc	17.567 ± 0.290	-2.742 ± 0.684	0.094	20
	All	17.858 ± 0.031	-2.880 ± 0.139	0.094	191
W_{H,K_s}	RRab	18.327 ± 0.048	-2.440 ± 0.232	0.085	156
	RRc	17.754 ± 0.217	-3.169 ± 0.515	0.097	20
	All	18.254 ± 0.032	-2.814 ± 0.145	0.090	192
W_{J,K_s}	RRab	18.121 ± 0.032	-2.667 ± 0.153	0.061	161
	RRc	17.522 ± 0.193	-3.377 ± 0.452	0.081	22
	All	18.069 ± 0.023	-2.942 ± 0.102	0.066	198

NOTE—The zero-point (a), slope (b), dispersion (σ) and the number of stars (N) in the final PL fits are tabulated.

were adopted to calibrate the zero-points of corresponding ACEP PL relations for a relative comparison.

The bottom panel of Fig. 6 displays K_s -band PL relation for ACEP in Draco dSph and the LMC. The figure shows that four ACEP in our sample occupy the location along the PL relation for fundamental mode variables while one ACEP is an overtone variable. The first-overtone ACEP (DR3-1433153827020071168) was also found to follow V -band PL relation of overtone mode pulsators in Kinemuchi et al. (2008), but the larger scatter in optical bands precluded authors to confirm its sub-classification. The tight PL relations in NIR allow us to confirm that this ACEP is pulsating in the first-overtone mode. The four fundamental mode ACEP fall along a linear sequence and cover a period range of $\Delta \log(P) \sim 0.45$ days. This period range is sufficient to derive PL relations in JHK_s bands which are also shown in Fig. 6. The results of the best-fitting PL relations in the form of equation (1) are tabulated in Table 4. Despite the small sample size, the slope of ACEP PL relation in the K_s -band agrees well with the slope of fundamental-mode PL relation in the LMC (-3.54 ± 0.15 , Ripepi et al. 2014).

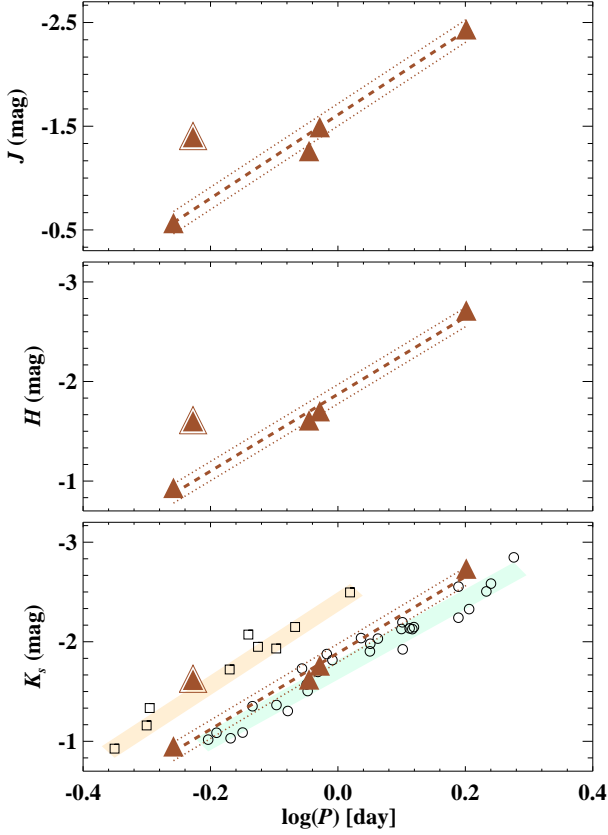


Figure 6. Near-infrared period-luminosity relations for ACEP (triangles) in J (top), H (middle), and K_s (bottom). In the bottom panel, open circles and squares represent fundamental and first-overtone mode ACEP in the LMC, respectively, and the shaded regions represent their PL relations with $\pm 1\sigma$ scatter (Ripepi et al. 2014). The dashed-lines represent best-fitting PL relation to four ACEP pulsating in the fundamental mode while the dotted lines display $\pm 2.5\sigma$ offsets from the best-fitting relation. The first-overtone mode ACEP is marked with overplotted open triangle.

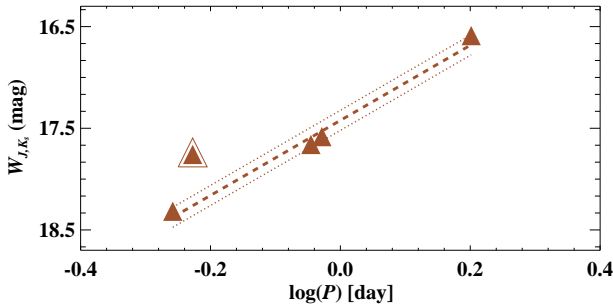


Figure 7. Same as Fig. 6, but for W_{J,K_s} period-Wesenheit relation for ACEP stars.

Table 4. Near-infrared PL and PW relations of ACEP stars in Draco dSph.

Band	Type	a_λ	b_λ	σ	N
J	ACEP-F	17.940 ± 0.031	-4.029 ± 0.149	0.108	4
H	ACEP-F	17.677 ± 0.037	-3.865 ± 0.231	0.097	4
K_s	ACEP-F	17.643 ± 0.034	-3.832 ± 0.207	0.092	4
$W_{J,H}$	ACEP-F	17.145 ± 0.057	-3.464 ± 0.272	0.186	4
W_{H,K_s}	ACEP-F	17.615 ± 0.044	-3.901 ± 0.275	0.112	4
W_{J,K_s}	ACEP-F	17.422 ± 0.036	-3.692 ± 0.218	0.099	4

NOTE—The zero-point (a), slope (b), dispersion (σ) and the number of stars (N) in the final PLR fits are tabulated.

The calibrated zero-points of fundamental-mode ACEP PL relations in the Draco dSph and the LMC are systematically different as seen in the bottom panel of Fig. 6. With above-mentioned distance to the Draco dSph, the absolute zero-point of -1.887 ± 0.078 mag is 0.17 magnitude brighter than that of ACEP in the LMC (Ripepi et al. 2014). We note that the slopes of these relations also differ by ~ 0.3 mag/dex, but are consistent within 1.2σ of their combined uncertainties. Recently, the first spectroscopic observations of Galactic ACEP stars by Ripepi et al. (2023) have confirmed that these are metal-poor stars ($[\text{Fe}/\text{H}] < -1.5$ dex), but their metallicities are not known in the LMC and Draco dSph. For RRL stars, the mean $[\text{Fe}/\text{H}]$ values in the LMC (~ -1.5 dex, Gratton et al. 2004; Borissova et al. 2009) and the Draco dSph (~ -2.0 dex, Muraveva et al. 2020) are comparatively different with the latter being more metal-poor. Similar to RRL stars, the mean metallicities of ACEP in the LMC and Draco dSph are also expected to be significantly different. Therefore, the difference in the zero-points may hint at a possible metallicity effect on their PL relations such that the more metal-poor stars are fainter. Assuming a metallicity difference of $\Delta[\text{Fe}/\text{H}] = 0.5$ dex between LMC and Draco, a zero-point offset of 0.17 mag would imply a negative metallicity term of the order of ~ -0.34 mag/dex. This value falls in the range of metallicity coefficients of NIR PL relations for more popular classical Cepheids in several recent studies (e.g., Bhardwaj et al. 2023b; Trentin et al. 2023).

Fig. 7 displays the W_{J,K_s} band PW relation for ACEP variables. The coefficients of all Wesenheit relations are tabulated in Table 4. Similar to RRL stars, the scatter increases in the PW relations in $W_{J,H}$ and W_{H,K_s} bands. We note that there are no NIR PW relations for ACEP stars in the literature for a relative comparison.

Table 5. Distance modulus estimates to Draco dSph galaxy.

μ (mag)	[Fe/H] (dex)	$E(B - V)$ (mag)	Method	Reference
19.55±0.03	-1.98±0.10	0.027	RRL PLZ $_{K_s}$ relation	TW
19.55±0.03	-1.98±0.10	0.027	RRL PLZ $_H$ relation	TW
19.64±0.04	-1.98±0.10	0.027	RRL PLZ $_J$ relation	TW
19.43±0.06	—	0.027	ACEP PL $_{K_s}$ relation	TW
19.39±0.03 ^a	-2.00± —	—	PWZ $_{VI}$ relation	Nagarajan et al. (2022)
19.53±0.07	-1.98±0.01	0.027	RRL M_G -[Fe/H] relation	Muraveva et al. (2020)
19.35±0.12	—	—	Density model fitting	Hernitschek et al. (2019)
19.51±0.03 ^a	—	—	PLZ $_i$ relation	Sesar et al. (2017)
19.58±0.15	-2.19±0.03	0.027	RRL M_V -[Fe/H] relation	Kinemuchi et al. (2008)
19.49±—	—	0.027	ACEP PL $_V$ relation	Kinemuchi et al. (2008)
19.49±0.15	—	0.03	TRGB	Cioni & Habing (2005)
19.40±0.15	-2.00±—	0.027	RRL M_V -[Fe/H] relation	Bonanos et al. (2004)
19.84±0.14	—	0.03	M_V Horizontal Branch stars	Bellazzini et al. (2002)
19.5±0.2	—	0.03	M_V Horizontal Branch stars	Aparicio et al. (2001)
19.6±0.3	—	0.03	M_V RRd stars	Nemec (1985)
19.4±0.3	—	0.03	M_V Horizontal Branch stars	Stetson (1979)
$\mu_{\text{Draco}} = 19.557 \pm 0.026$ (stat.) ± 0.031 (syst.) mag				TW
$D_{\text{Draco}} = 81.545 \pm 0.977$ (stat.) ± 1.165 (syst.) kpc				TW

NOTE—We adopted an uncertainty of 0.1 dex in mean metallicity from Kirby et al. (2013).

^aSee the text in Section 5.

5. DISTANCE TO DRACO DSPH USING POPULATION II STARS

Draco is one of the nearest satellites of the Milky Way. Yet, its distance is not very accurate despite several detailed studies of resolved stellar populations. Table 5 lists distance moduli measurements to Draco dSph available in the literature. It is evident that the distance modulus varies between 19.35 ± 0.03 mag and 19.84 ± 0.14 mag in studies based on modern photometric data. The majority of these measurements are based on visual magnitude of horizontal branch stars or traditional M_V -[Fe/H] relation for RRL stars. These empirical relations suffer from evolutionary effects, and extinction and metallicity uncertainties, as mentioned in the Section 1, and therefore exhibit larger realistic uncertainties of 0.1 – 0.2 mag. Regardless, the resulting distance moduli typically range between 19.50 and 19.60 mag, except for the measurement from Bellazzini et al. (2002), which is at the high end with 19.84 mag. Two recent distance moduli estimates based on RRL density model fitting (Hernitschek et al. 2019) and optical PWZ relation (Nagarajan et al. 2022) are smaller than 19.40 mag. Nagarajan et al. (2022) employed global fits to heterogeneous optical data for RRL stars and quoted a rather small statistical uncertainty of 0.03 mag, which

presumably does not include any calibration errors since the uncertainty on their adopted PWZ zero-point itself is ~ 0.05 mag. Similarly, Sesar et al. (2017) quoted a small uncertainty of only 0.03 mag on distance modulus. The authors assumed a Gaussian metallicity distribution centered on -1.5 dex with a standard deviation of 0.3 dex for the RRL stars, which is different from most other studies, including this work. The quoted error only includes adopted error on absolute i -band magnitudes, excluding possible reddening and metallicity uncertainties in the calibration.

5.1. RRL and ACEP variables

We utilized accurate and precise PL relations for RR Lyrae stars in Draco dSph to determine its distance modulus. The calibrator PLZ relations in NIR bands were adopted from Bhardwaj et al. (2023a), who provided the most precise empirical determination of the metallicity coefficient using homogeneous NIR photometry of ~ 1000 RRL in 11 globular clusters. The authors found that these empirical PLZ relations are in good agreement with theoretical predictions (Catelan et al. 2004; Marconi et al. 2015). The adopted calibrations and the observations presented in this work were obtained with the same instrument/telescope and with

similar methodology, thus mitigating any possible analysis systematic uncertainties.

To apply these empirical and theoretical calibrations, we need to assume a mean metallicity for RRL stars in Draco. [Muraveva et al. \(2020\)](#) identified 16 RRL variables with spectroscopic metallicity measurements from [Walker et al. \(2015\)](#) with a mean metallicity of -1.98 ± 0.65 dex. [Walker et al. \(2015\)](#) derived $[\text{Fe}/\text{H}]$ values of red giant and horizontal branch stars in Draco with a median uncertainty of 0.20 dex, but the errors range between 0.06 and 0.98 dex for bright and faint stars. The large scatter of 0.65 dex in the mean metallicity of 16 RRL stars is likely due to larger uncertainties in the individual $[\text{Fe}/\text{H}]$ measurements of horizontal branch stars. Nevertheless, this mean $[\text{Fe}/\text{H}]$ value is in agreement with the mean metallicity of Draco of -1.98 ± 0.01 dex ($\sigma = 0.42$ dex) from [Kirby et al. \(2013\)](#) based on spectroscopic observations of its members. Recently, [Taibi et al. \(2022\)](#) derived a metallicity of -1.86 for Draco mainly using the red giant branch stars. Since the dispersion in NIR PL relations suggests a small scatter in metallicity, we adopted a mean metallicity of -1.98 ([Kirby et al. 2013](#)) with assumed error of 0.10 dex for Draco dSph.

The distance modulus measurements based on RRL PL relations are listed in Table 5. In the HK_s -band, the distance moduli are 19.55 ± 0.03 mag with a systematic error of 0.03 mag. The distance modulus is $\sim 2\sigma$ larger in the J -band. We note that the absolute zero-points in the J -band differ by 0.06 mag between empirical and theoretical calibrations ([Bhardwaj et al. 2023b](#)), while they agree within 0.02 mag in the HK_s bands. The larger uncertainties in the J -band PLZ calibrations may be contributing to a relatively larger distance modulus. The uncertainties on the coefficients of the calibrator PLZ relations and the empirical PL relations were propagated to determine statistical errors. The systematic errors include the uncertainties on the zero-points of the calibrator PLZ relation ($\sim 0.02 - 0.03$ mag) and empirical PL relation (~ 0.02 mag), and the uncertainty due to 0.1 dex variation in the mean metallicity or metallicity scale (~ 0.02 mag). The errors due to reddening are negligible (< 0.005 mag) considering small color-excess value and extinction coefficients in the NIR.

We also determined RRL based distances adopting independent theoretical PLZ calibrations from [Marconi et al. \(2015\)](#) in NIR bands. These distance moduli derivations agree well within 1σ with the quoted values in Table 5 based on empirical calibrations. Due to larger scatter in the Wesenheit relations for Draco RRL and their empirical calibrations, we do not use those to determine distance modulus. Exclud-

ing relatively larger J -band determinations, we adopt a weighted average of distance moduli based on HK_s band for both empirical and theoretical calibrations. Our recommended distance modulus to Draco dSph is 19.557 ± 0.026 (stat.) ± 0.031 (syst.) mag, which translates to a distance of 81.55 ± 0.98 (stat.) ± 1.17 (syst.) kpc.

Our small sample of 5 ACEPs can also be used to determine an independent distance to Draco dSph. Only fundamental mode ACEPs were used for this analysis excluding one of the overtone mode variable. The empirically calibrated K_s -band PL relation for ACEPs in the LMC ([Ripepi et al. 2014](#)) was used to determine absolute magnitude for Draco variables. The resulting distance modulus of 19.43 ± 0.06 mag based on ACEPs is also listed in Table 5. This distance modulus is smaller than the adopted RRL based determination, but is in agreement within 2σ of their quoted uncertainties. There are no other absolute calibrations of PL and PW relations in the NIR bands for ACEP stars.

Thanks to unprecedented NIR photometry, our RRL distance measurements are significantly more precise and accurate, but also agree well with most previous determinations in the literature. The adopted calibrations and the observations presented in this work were obtained with the same telescope, same instrument and filters, as well as the same methodology applied for data reduction and measurements analysis, thus minimising any possible systematic uncertainties.

5.2. Tip of the red giant branch

Among population II distance indicators, the tip of the red giant (TRGB) is significantly brighter than RRL stars, and is an excellent distance indicator. In particular, the I -band magnitude of TRGB is remarkably constant over a range of metallicities, but their magnitude distribution is slanted or sloped with increasing metallicity at other wavelengths ([Lee et al. 1993](#); [Rizzi et al. 2007](#); [Serenelli et al. 2017](#); [Freedman et al. 2020](#)). [Cioni & Habing \(2005\)](#) measured a TRGB-based distance of 19.49 ± 0.06 (stat.) ± 0.15 (syst.) to Draco dsph. Despite a relatively small number of red giant branch stars near the TRGB, the authors utilized more than a minimum of 100 stars - a criterion suggested by [Madore & Freedman \(1995\)](#) for a robust determination of the TRGB magnitude. Recently, [Madore et al. \(2023\)](#) suggested that a population of ~ 100 RGB stars is insufficient to provide reliable measurement of the TRGB magnitude.

We derived optical and NIR color-magnitude diagrams to determine an independent TRGB-based distance to Draco dSph. Although, [Kinemuchi et al. \(2008\)](#)

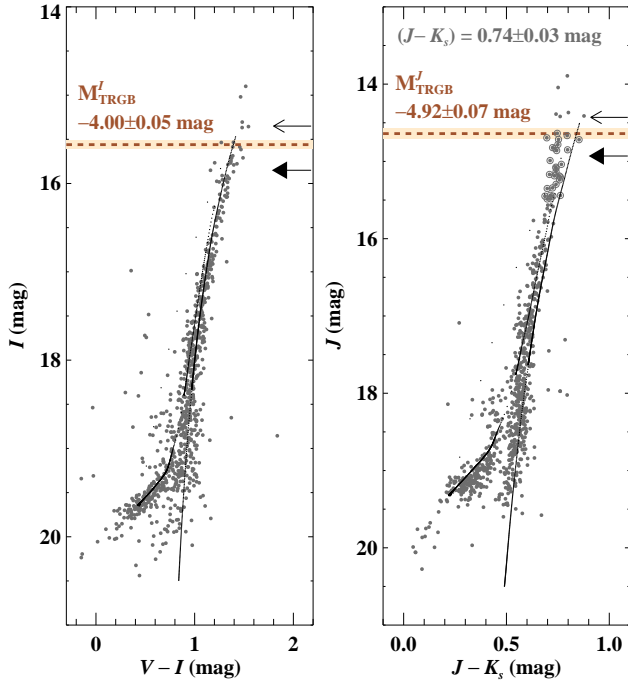


Figure 8. Optical and NIR color–magnitude diagrams for the proper motion cleaned members of Draco dSph. *Left:* $V - I, I$ color–magnitude diagram. *Right:* $J - K_s, J$ color–magnitude diagram. The overplotted open circles represent red giants used to determine average color, $J - K_s = 0.74 \pm 0.03$ mag, for TRGB measurement. The dashed lines represent the location of TRGB in Draco dSph in the optical and NIR and the shaded regions display their $\pm 1\sigma$ uncertainties. The dotted lines show BaSTI stellar isochrones (Pietrinferni et al. 2021) with 10 Gyr age and metallicity of Draco dSph. The open and filled arrows display the expected location of TRGB corresponding to the distance modulus of 19.35 and 19.85 mag, respectively. These are the upper and lower limit of the distance moduli for Draco in the recent literature studies (see text).

provided optical VI -band photometry for variables in Draco, we used homogeneous *Gaia* photometry of ~ 7000 sources within $30'$ around the center of Draco for this analysis. The G -band magnitudes and (BP–RP) colors were used in the *Gaia* to Johnson-Cousin photometric transformations from Pancino et al. (2022) to derive V and I band magnitudes. We apply proper motion cleaning as previously discussed in Section 3.2 for the NIR data. The extinction-correction in the V and I bands were estimated using $R_{V/I} = 3.23/1.97E(B - V)$ to be consistent with the coefficients adopted in the NIR bands. The optical and NIR color–magnitude diagrams are shown in Fig. 8. It is clearly evident that the number of RGB stars one-magnitude below the TRGB is very small, preventing an accurate and precise measurement of TRGB magnitude.

Nevertheless, the color–magnitude diagrams shown in Fig. 8 provide an opportunity to independently verify the accuracy of RRL-based distance to Draco dSph derived in this work. In the I -band, we adopted an absolute TRGB magnitude of -4.00 ± 0.05 mag, which covers the range of most recent calibrations in the literature (e.g., Freedman et al. 2020; Li et al. 2023; Dixon et al. 2023, and references therein). In the NIR bands, the J -band TRGB magnitude was derived using $M_J = 5.14 - 0.85[(J - K_s) - 1.0]$ from Freedman et al. (2020). We used an average color $(J - K_s) = 0.74 \pm 0.03$, using red giant stars in a magnitude-bin below the approximate location of the TRGB in Fig. 8, and found a value of $M_{\text{TRGB}}^J = -4.92 \pm 0.07$ mag. The apparent TRGB magnitude in I and J bands were derived using the above-mentioned absolute magnitudes and the RRL-based distance modulus to Draco dSph. In the color–magnitude diagrams, the discontinuity at the TRGB is clearly visible and is in excellent agreement with the derived apparent TRGB magnitudes in the optical and NIR bands, as shown with dashed lines in Fig. 8. Adopting a significantly larger or smaller distance to Draco dSph results in an offset from the apparent discontinuity in the color–magnitude diagram. We also overplot the stellar isochrones from BaSTI³ (Bag of Stellar Tracks and Isochrones) for a constant age of 10 Gyr and metallicity of $Z = 0.0004$ ($[\text{Fe}/\text{H}] = -1.90$ dex), and $Y = 0.245$ using models with α -enhanced calculations from Pietrinferni et al. (2021). The stellar isochrones were offset with the RRL distance and show a reasonable agreement with the apparent location of the TRGB in Draco dSph. This further confirms the accuracy of the distance derived in this work and the consistency among population II distance indicators in Draco dSph galaxy.

6. SUMMARY

We presented NIR time-series observations of pulsating variable stars in Draco dSph galaxy for the first-time. These observations were obtained using the WIRCam instrument at the 3.6-m Canada–France–Hawaii Telescope. Homogeneous NIR light curves of 212 RRL and 5 ACEP variables were fitted with templates resulting in accurate mean magnitudes in JHK_s bands. We derived NIR PL relations for different subclasses of RRL stars and fundamental mode ACEP variables for the first-time in Draco dSph. The empirical PL relations for RRL stars exhibit a small scatter of ~ 0.05 mag in JHK_s bands that is comparable to those seen for RRL PL relations in globular clusters. The low dis-

³ <http://basti-iac.oa-abruzzo.inaf.it/index.html>

persion of PL relation in NIR bands suggests at most about 0.2 dex spread in the metallicity of RRL stars in Draco dSph. We adopted a mean metallicity of -1.98 ± 0.10 dex (Kirby et al. 2013) and calibrated NIR PLZ relations from Bhardwaj et al. (2023a) to determine distance modulus of 19.56 ± 0.03 mag to Draco dSph. The final distance to Draco $D_{\text{Draco}} = 81.55 \pm 0.98(\text{statistical}) \pm 1.17(\text{systematic})$ kpc, is 1.5% precise and the most accurate distance to this dSph galaxy. Using this RRL distance, the absolute magnitudes of the TRGB in I and J bands in the optical and NIR color–magnitude diagrams, respectively, agree well with their recent calibrations in the literature. However, a low number of red giant stars within the one magnitude of the TRGB prevents an accurate and precise determination of its magnitude, and in turn, an independent distance to Draco dSph. This paper is the first in a series that will provide time-series observations of pulsating variable stars in nearby galaxies. Precise RRL based distances to several nearby dwarf galaxies will allow an independent calibration of the TRGB, and a crucial test for the population II distance scale.

ACKNOWLEDGMENTS

We thank Dr. Tatiana Muraveva for kindly providing the variable star list in Draco dSph galaxy. This project has received funding from the European Union’s Horizon 2020 research and innovation programme under the Marie Skłodowska-Curie grant agreement No. 886298. This research was supported by the Munich Institute for Astro-, Particle and BioPhysics (MIAPbP) which is funded by the Deutsche Forschungsgemeinschaft (DFG, German Research Foundation) under Germany’s Excellence Strategy – EXC-2094 – 390783311. CCN thanks the funding from the National Science and Technology Council (NSTC; Taiwan) under the contract 109-2112-M-008-014-MY3 and 112-2112-M-008-042. Access to the CFHT was made possible by the Institute of Astronomy and Astrophysics, Academia Sinica.

Facility: CFHT-WIRCAM

Software: The IDL Astronomy User’s Library (Landsman 1993), Astropy (Astropy Collaboration et al. 2013, 2018, 2022), Libre-ESpRIT (Donati et al. 1997)

REFERENCES

- Aaronson, M. 1983, ApJ, 266, L11, doi: [10.1086/183969](https://doi.org/10.1086/183969)
- Aparicio, A., Carrera, R., & Martínez-Delgado, D. 2001, AJ, 122, 2524, doi: [10.1086/323535](https://doi.org/10.1086/323535)
- Astropy Collaboration, Robitaille, T. P., Tollerud, E. J., et al. 2013, A&A, 558, A33, doi: [10.1051/0004-6361/201322068](https://doi.org/10.1051/0004-6361/201322068)
- Astropy Collaboration, Price-Whelan, A. M., Sipőcz, B. M., et al. 2018, AJ, 156, 123, doi: [10.3847/1538-3881/aabc4f](https://doi.org/10.3847/1538-3881/aabc4f)
- Astropy Collaboration, Price-Whelan, A. M., Lim, P. L., et al. 2022, ApJ, 935, 167, doi: [10.3847/1538-4357/ac7c74](https://doi.org/10.3847/1538-4357/ac7c74)
- Baade, W., & Swope, H. H. 1961, AJ, 66, 300, doi: [10.1086/108431](https://doi.org/10.1086/108431)
- Battaglia, G., & Nipoti, C. 2022, Nature Astronomy, 6, 659, doi: [10.1038/s41550-022-01638-7](https://doi.org/10.1038/s41550-022-01638-7)
- Beaton, R. L., Bono, G., Braga, V. F., et al. 2018, Space Science Reviews, 214, 113, doi: [10.1007/s11214-018-0542-1](https://doi.org/10.1007/s11214-018-0542-1)
- Bellazzini, M., Ferraro, F. R., Origlia, L., et al. 2002, AJ, 124, 3222, doi: [10.1086/344794](https://doi.org/10.1086/344794)
- Bertin, E. 2006, in Astronomical Society of the Pacific Conference Series, Vol. 351, Astronomical Data Analysis Software and Systems XV, ed. C. Gabriel, C. Arviset, D. Ponz, & S. Enrique, 112
- Bertin, E., & Arnouts, S. 1996, Astronomy and Astrophysics Supplement, 117, 393, doi: [10.1051/aas:1996164](https://doi.org/10.1051/aas:1996164)
- Bertin, E., Mellier, Y., Radovich, M., et al. 2002, in Astronomical Society of the Pacific Conference Series, Vol. 281, Astronomical Data Analysis Software and Systems XI, ed. D. A. Bohlender, D. Durand, & T. H. Handley, 228
- Bhardwaj, A. 2020, Journal of Astrophysics and Astronomy, 41, 23, doi: [10.1007/s12036-020-09640-z](https://doi.org/10.1007/s12036-020-09640-z)
- . 2022, Universe, 8, 122, doi: [10.3390/universe8020122](https://doi.org/10.3390/universe8020122)
- Bhardwaj, A., Rejkuba, M., de Grijs, R., et al. 2020, AJ, 160, 220, doi: [10.3847/1538-3881/abb3f9](https://doi.org/10.3847/1538-3881/abb3f9)
- Bhardwaj, A., Rejkuba, M., Sloan, G. C., Marconi, M., & Yang, S.-C. 2021a, ApJ, 922, 20, doi: [10.3847/1538-4357/ac214d](https://doi.org/10.3847/1538-4357/ac214d)
- Bhardwaj, A., Rejkuba, M., de Grijs, R., et al. 2021b, ApJ, 909, 200, doi: [10.3847/1538-4357/abdf48](https://doi.org/10.3847/1538-4357/abdf48)
- Bhardwaj, A., Marconi, M., Rejkuba, M., et al. 2023a, ApJL, 944, L51, doi: [10.3847/2041-8213/acba7f](https://doi.org/10.3847/2041-8213/acba7f)
- Bhardwaj, A., Riess, A. G., Catanzaro, G., et al. 2023b, ApJL, 955, L13, doi: [10.3847/2041-8213/acf710](https://doi.org/10.3847/2041-8213/acf710)
- Bonanos, A. Z., Stanek, K. Z., Szentgyorgyi, A. H., Sasselov, D. D., & Bakos, G. Á. 2004, AJ, 127, 861, doi: [10.1086/381073](https://doi.org/10.1086/381073)
- Borissova, J., Rejkuba, M., Minniti, D., Catelan, M., & Ivanov, V. D. 2009, A&A, 502, 505, doi: [10.1051/0004-6361/200811465](https://doi.org/10.1051/0004-6361/200811465)

- Braga, V. F., Stetson, P. B., Bono, G., et al. 2019, *A&A*, 625, A1, doi: [10.1051/0004-6361/201834893](https://doi.org/10.1051/0004-6361/201834893)
- Braga, V. F., Fiorentino, G., Bono, G., et al. 2022, *MNRAS*, 517, 5368, doi: [10.1093/mnras/stac2813](https://doi.org/10.1093/mnras/stac2813)
- Bullock, J. S., & Boylan-Kolchin, M. 2017, *ARA&A*, 55, 343, doi: [10.1146/annurev-astro-091916-055313](https://doi.org/10.1146/annurev-astro-091916-055313)
- Caputo, F., Castellani, V., Marconi, M., & Ripepi, V. 2000, *MNRAS*, 316, 819, doi: [10.1046/j.1365-8711.2000.03591.x](https://doi.org/10.1046/j.1365-8711.2000.03591.x)
- Cardelli, J. A., Clayton, G. C., & Mathis, J. S. 1989, *ApJ*, 345, 245, doi: [10.1086/167900](https://doi.org/10.1086/167900)
- Catelan, M., Pritzl, B. J., & Smith, H. A. 2004, *ApJS*, 154, 633, doi: [10.1086/422916](https://doi.org/10.1086/422916)
- Cioni, M. R. L., & Habing, H. J. 2005, *A&A*, 442, 165, doi: [10.1051/0004-6361:20053368](https://doi.org/10.1051/0004-6361:20053368)
- Coppola, G., Marconi, M., Stetson, P. B., et al. 2015, *ApJ*, 814, 71, doi: [10.1088/0004-637X/814/1/71](https://doi.org/10.1088/0004-637X/814/1/71)
- Dixon, M., Mould, J., Flynn, C., et al. 2023, *MNRAS*, 523, 2283, doi: [10.1093/mnras/stad1500](https://doi.org/10.1093/mnras/stad1500)
- Donati, J. F., Semel, M., Carter, B. D., Rees, D. E., & Collier Cameron, A. 1997, *MNRAS*, 291, 658, doi: [10.1093/mnras/291.4.658](https://doi.org/10.1093/mnras/291.4.658)
- Freedman, W. L., Madore, B. F., Hoyt, T., et al. 2020, *ApJ*, 891, 57, doi: [10.3847/1538-4357/ab7339](https://doi.org/10.3847/1538-4357/ab7339)
- Gaia Collaboration, Vallenari, A., Brown, A. G. A., et al. 2023, *A&A*, 674, A1, doi: [10.1051/0004-6361/202243940](https://doi.org/10.1051/0004-6361/202243940)
- Gieren, W., Pietrzyński, G., Soszyński, I., et al. 2005, *ApJ*, 628, 695, doi: [10.1086/430903](https://doi.org/10.1086/430903)
- Gratton, R. G., Bragaglia, A., Clementini, G., et al. 2004, *A&A*, 421, 937, doi: [10.1051/0004-6361:20035840](https://doi.org/10.1051/0004-6361:20035840)
- Grebel, E. K., Gallagher, John S., I., & Harbeck, D. 2003, *AJ*, 125, 1926, doi: [10.1086/368363](https://doi.org/10.1086/368363)
- Grillmair, C. J., Mould, J. R., Holtzman, J. A., et al. 1998, *AJ*, 115, 144, doi: [10.1086/300169](https://doi.org/10.1086/300169)
- Hernitschek, N., Cohen, J. G., Rix, H.-W., et al. 2019, *ApJ*, 871, 49, doi: [10.3847/1538-4357/aaf388](https://doi.org/10.3847/1538-4357/aaf388)
- Karczmarek, P., Pietrzyński, G., Gieren, W., et al. 2021, *ApJS*, 253, 42, doi: [10.3847/1538-4365/abdf60](https://doi.org/10.3847/1538-4365/abdf60)
- Kinemuchi, K., Harris, H. C., Smith, H. A., et al. 2008, *AJ*, 136, 1921, doi: [10.1088/0004-6256/136/5/1921](https://doi.org/10.1088/0004-6256/136/5/1921)
- Kirby, E. N., Cohen, J. G., Guhathakurta, P., et al. 2013, *ApJ*, 779, 102, doi: [10.1088/0004-637X/779/2/102](https://doi.org/10.1088/0004-637X/779/2/102)
- Landsman, W. B. 1993, in *ASP Conference Series*, Vol. 52, *Astronomical Data Analysis Software and Systems II*, ed. R. J. Hanisch, R. J. V. Brissenden, & J. Barnes, 246
- Lee, M. G., Freedman, W. L., & Madore, B. F. 1993, *ApJ*, 417, 553, doi: [10.1086/173334](https://doi.org/10.1086/173334)
- Li, S., Casertano, S., & Riess, A. G. 2023, *ApJ*, 950, 83, doi: [10.3847/1538-4357/accd69](https://doi.org/10.3847/1538-4357/accd69)
- Longmore, A. J., Fernley, J. A., & Jameson, R. F. 1986, *MNRAS*, 220, 279, doi: [10.1093/mnras/220.2.279](https://doi.org/10.1093/mnras/220.2.279)
- Madore, B. F. 1982, *ApJ*, 253, 575, doi: [10.1086/159659](https://doi.org/10.1086/159659)
- Madore, B. F., & Freedman, W. L. 1995, *AJ*, 109, 1645, doi: [10.1086/117391](https://doi.org/10.1086/117391)
- Madore, B. F., Freedman, W. L., Owens, K. A., & Jang, I. S. 2023, *AJ*, 166, 2, doi: [10.3847/1538-3881/acd3f3](https://doi.org/10.3847/1538-3881/acd3f3)
- Marconi, M., Coppola, G., Bono, G., et al. 2015, *ApJ*, 808, 50, doi: [10.1088/0004-637X/808/1/50](https://doi.org/10.1088/0004-637X/808/1/50)
- Marmo, C., & Bertin, E. 2008, in *Astronomical Society of the Pacific Conference Series*, Vol. 394, *Astronomical Data Analysis Software and Systems XVII*, ed. R. W. Argyle, P. S. Bunclark, & J. R. Lewis, 619
- Massari, D., Helmi, A., Mucciarelli, A., et al. 2020, *A&A*, 633, A36, doi: [10.1051/0004-6361/201935613](https://doi.org/10.1051/0004-6361/201935613)
- Mateo, M. L. 1998, *ARA&A*, 36, 435, doi: [10.1146/annurev.astro.36.1.435](https://doi.org/10.1146/annurev.astro.36.1.435)
- McConnachie, A. W. 2012, *AJ*, 144, 4, doi: [10.1088/0004-6256/144/1/4](https://doi.org/10.1088/0004-6256/144/1/4)
- Monelli, M., & Fiorentino, G. 2022, *Universe*, 8, 191, doi: [10.3390/universe8030191](https://doi.org/10.3390/universe8030191)
- Muraveva, T., Clementini, G., Garofalo, A., & Cusano, F. 2020, *MNRAS*, 499, 4040, doi: [10.1093/mnras/staa2984](https://doi.org/10.1093/mnras/staa2984)
- Nagarajan, P., Weisz, D. R., & El-Badry, K. 2022, *ApJ*, 932, 19, doi: [10.3847/1538-4357/ac69e6](https://doi.org/10.3847/1538-4357/ac69e6)
- Nemec, J. M. 1985, *AJ*, 90, 204, doi: [10.1086/113727](https://doi.org/10.1086/113727)
- Pace, A. B., Erkal, D., & Li, T. S. 2022, *ApJ*, 940, 136, doi: [10.3847/1538-4357/ac997b](https://doi.org/10.3847/1538-4357/ac997b)
- Pancino, E., Marrese, P. M., Marinoni, S., et al. 2022, *A&A*, 664, A109, doi: [10.1051/0004-6361/202243939](https://doi.org/10.1051/0004-6361/202243939)
- Pietrinferni, A., Hidalgo, S., Cassisi, S., et al. 2021, *ApJ*, 908, 102, doi: [10.3847/1538-4357/abd4d5](https://doi.org/10.3847/1538-4357/abd4d5)
- Pietrzyński, G., Graczyk, D., Gellenne, A., et al. 2019, *Nature*, 567, 200, doi: [10.1038/s41586-019-0999-4](https://doi.org/10.1038/s41586-019-0999-4)
- Puget, P., Stadler, E., Doyon, R., et al. 2004, in *Society of Photo-Optical Instrumentation Engineers (SPIE) Conference Series*, Vol. 5492, *Ground-based Instrumentation for Astronomy*. Edited by Alan F. M. Moorwood and Iye Masanori. Proceedings of the SPIE, ed. A. F. M. Moorwood & M. Iye, 978–987, doi: [10.1117/12.551097](https://doi.org/10.1117/12.551097)
- Read, J. I., Walker, M. G., & Steger, P. 2018, *MNRAS*, 481, 860, doi: [10.1093/mnras/sty2286](https://doi.org/10.1093/mnras/sty2286)
- Ripepi, V., Marconi, M., Moretti, M. I., et al. 2014, *MNRAS*, 437, 2307, doi: [10.1093/mnras/stt2047](https://doi.org/10.1093/mnras/stt2047)
- Ripepi, V., Catanzaro, G., Trentin, E., et al. 2023, *arXiv e-prints*, arXiv:2310.20503, doi: [10.48550/arXiv.2310.20503](https://doi.org/10.48550/arXiv.2310.20503)
- Rizzi, L., Tully, R. B., Makarov, D., et al. 2007, *ApJ*, 661, 815, doi: [10.1086/516566](https://doi.org/10.1086/516566)
- Schlegel, D. J., Finkbeiner, D. P., & Davis, M. 1998, *ApJ*, 500, 525, doi: [10.1086/305772](https://doi.org/10.1086/305772)

- Ségall, M., Ibata, R. A., Irwin, M. J., Martin, N. F., & Chapman, S. 2007, *MNRAS*, 375, 831, doi: [10.1111/j.1365-2966.2006.11356.x](https://doi.org/10.1111/j.1365-2966.2006.11356.x)
- Serenelli, A., Weiss, A., Cassisi, S., Salaris, M., & Pietrinferni, A. 2017, *A&A*, 606, A33, doi: [10.1051/0004-6361/201731004](https://doi.org/10.1051/0004-6361/201731004)
- Sesar, B., Hernitschek, N., Mitrović, S., et al. 2017, *AJ*, 153, 204, doi: [10.3847/1538-3881/aa661b](https://doi.org/10.3847/1538-3881/aa661b)
- Skrutskie, M. F., Cutri, R. M., Stiening, R., et al. 2006, *AJ*, 131, 1163, doi: [10.1086/498708](https://doi.org/10.1086/498708)
- Stetson, P. B. 1979, *AJ*, 84, 1149, doi: [10.1086/112522](https://doi.org/10.1086/112522)
- . 1987, *PASP*, 99, 191, doi: [10.1086/131977](https://doi.org/10.1086/131977)
- . 1994, *PASP*, 106, 250, doi: [10.1086/133378](https://doi.org/10.1086/133378)
- Taibi, S., Battaglia, G., Leaman, R., et al. 2022, *A&A*, 665, A92, doi: [10.1051/0004-6361/202243508](https://doi.org/10.1051/0004-6361/202243508)
- Tolstoy, E., Hill, V., & Tosi, M. 2009, *ARA&A*, 47, 371, doi: [10.1146/annurev-astro-082708-101650](https://doi.org/10.1146/annurev-astro-082708-101650)
- Trentin, E., Ripepi, V., Molinaro, R., et al. 2023, arXiv e-prints, arXiv:2310.03603, doi: [10.48550/arXiv.2310.03603](https://doi.org/10.48550/arXiv.2310.03603)
- Walker, M. G., Olszewski, E. W., & Mateo, M. 2015, *MNRAS*, 448, 2717, doi: [10.1093/mnras/stv099](https://doi.org/10.1093/mnras/stv099)
- Zinn, R., & Searle, L. 1976, *ApJ*, 209, 734, doi: [10.1086/154772](https://doi.org/10.1086/154772)